Published in IET Electrical Systems in Transportation
Received on 9th November 2012
Revised on 25th March 2013
Accepted on 5th April 2013
doi: 10.1049/iet-est.2011.0056

ISSN 2042-9738

Mathematical analysis of the equivalent impedance at the harmonic frequency for the proposed aircraft power system

Qian Zhou, Mark Sumner, Dave Thomas

Department of Electrical and Electronics Engineering, University of Nottingham, Tower Building, University Park, Nottingham NG7 2RD, UK
E-mail: qian.zhou@nottingham.ac.uk

Abstract: The proposals for the 'More Electric Aircraft' place a significant, increased demand on the electrical power distribution system. To increase safety and reduce aircraft maintenance times on the ground, there is a greater need to quickly identify and locate electrical faults within the electrical distribution system. The work presented in this study provides the mathematical basis for the use of power system harmonic impedance measurement for identifying and locating faults within power cables. The method is passive – that is, it does not require the injection of any test signals – and can potentially be embedded into a centralised equipment controller to provide intelligent, real time diagnostics. The method monitors the harmonic line–line self-impedance at strategic points in the distribution system; this is obtained by measuring load voltage and current. Faults can be identified and located within a few fundamental cycles, and therefore provides a 'backup protection' system which does not require measurement of the line current. It also can provide details of the fault location and could therefore be a significant aid to aircraft maintenance. This study derives the theoretical basis of the scheme and provides simulation results for a proposed aircraft power system to demonstrate the validity of this approach to detect and locate faults within the system.

1 Introduction

The concept of the 'More Electric Aircraft' (MEA) has been introduced for overcoming certain drawbacks in conventional aircraft architectures and can bring many more attractive advantages [1, 2]. The demands of an MEA will increase the power distribution requirements of future aircraft electrical distribution systems. The increased reliance on electrical energy in an MEA puts increased stress on the protection and control systems, increasing the electrical energy distributed from a few hundred kW to over a MW for a 737 sized aircraft [2]. The introduction of the MEA emphasises the utilisation of electrical powers instead of pneumatic, mechanical and hydraulic powers. For the aircraft secondary power system, power electronic converters are required for most of the electric loads [3]. Improved fault identification, including the detection of a fault and its location, is important to enable the electrical power systems to meet the increased load demand and functionalities. The currently used protection schemes, for example, over-current, undervoltage and negative sequences, do not provide discrimination in an aircraft power system or could fail to operate because of component failure [4]. These traditional approaches may not be particularly accurate [5]. To increase safety accurately and reduce aircraft maintenance times on the ground, there is also a need to quickly identify and locate any electrical faults which may develop.

A large number of power electronic loads inject low order and switching harmonics into the system. Many previous simulation and experimental work were focused on an online system or load harmonic impedance measurement using transients associated with capacitor switching [6–12]. Yao *et al.* [13] applied voltage and current disturbances because of loads switching to take harmonic impedance measurement. In [14–16], a novel fault identification and location algorithm was proposed, which analysed the 'line–line self-impedance' at each load at the specific harmonic frequencies that were present in the system when an asymmetric fault occurred. The work formed an initial study into the use of power system harmonic impedance measurement for identifying and locating faults within power cables. The method required the phase voltages and line currents at different load distribution points within the system to be measured to estimate the harmonic line–line self-impedance at these strategic points in the distribution system. This method can be embedded into a centralised equipment controller to provide intelligent, real time diagnostics. By combining the harmonic line-line self-impedance estimates, the faults can be identified and located within a few fundamental cycles. This can therefore provide from overall the system a 'backup protection' system which does not require measurement of the line current. A measure of the fault location could also be a significant aid to aircraft maintenance.

In this paper, the mathematical analysis of the line-line self-impedance at the third harmonic frequency is

performed to support the findings of [14–16]. In [16], experimental work was presented to verify the capability of the line–line self-impedance at the third harmonic frequency for identifying fault location and providing information of fault resistance. This paper will provide an analytical solution for the line–line self-impedance at different strategic points that is related to fault resistance and fault location as represented in terms of cable characteristic parameters and cable length to the source terminal. Therefore the relationship of the line–line self-impedance at the third harmonic frequency to fault resistance and fault location, which are the two important aspects of fault identification, can be pre-described and applied as a powerful tool further to identify and locate faults.

This paper is organised as follows. Section 2 describes the example aircraft power system studied. Section 3 describes how the harmonic currents are produced using the rectifier switching functions and how they are related to a fault resistance and a fault location. Section 4 compares the results from the mathematical analysis with those obtained using the simulation method, which uses the block SIMPOWER in MATLAB/SIMULINK. Section 5 gives the conclusions.

2 Example aircraft power system

In this section, an example aircraft power system is described, which is a more realistic layout for MEA in comparison with that used in [14, 15]. The example system is shown in Fig. 1. The working frequency for the considered system is assumed to be a constant frequency, 400 Hz. The aircraft electrical system is unearthed so that only phase–phase faults are considered in this work.

The supply has an internal impedance of 0.001 Ω and 40 μH and is assumed to generate fundamental sinusoidal voltages. The nominal line voltage is 230 V rms. The characteristic parameters of cable resistance and inductance are 1.58 mΩ/m and 0.28 μH/m, respectively, which is typical cabling, used in aircraft. The system supplies three loads, the autotransformer rectifier unit (ATRU), the wing ice protection load (WIPS) and the electricmechanical actuator (EMA) load that is composed of an uncontrolled diode bridge rectifier and its equivalent DC load. In this paper, these three loads are numerically noted according to positions where they are connected within the system. For the load of ATRU, it is noted as Load 1. For the WIPS, it is noted as Load 2. The EMA load is noted as Load 3. The length of the cables supplying the ATRU load from the source terminal is 10 m; that of the cables supplying to the WIPS load is 5 m; the total length of the cables supplying to the EMA load is 30 m. This arrangement is typical of an aircraft system where the generators are directly mounted on the turbines and actuators are dispersed along the aircraft wings. The considered fault locations within the system are at every 5 m cable section as labelled as ' × ' in Fig. 1. The locations numbered as 1 and 2 are referred to cables connecting to the ARTU load. The fault location is numbered as 3 for cables connecting to WIPS load. The considered fault locations for cables connecting to the EMA load are numbered as 4–9 from the source terminal to the EMA load.

In this paper, the ATRU load is simplified and modelled as a three-phase inductive load, which has a nominal power of 100 kW with a power factor of 0.9. The WIPS load is modelled as a three-phase pure resistive load, which has a nominal power of 125 kW. The line inductor connected to the input terminal of the uncontrolled diode bridge rectifier (EMA) has the inductance of 10 μH. This is a typical filter value. Its DC load resistance and inductance are 3.844 Ω and 3.1 mH, respectively. In the following analysis, the EMA is the only non-linear load.

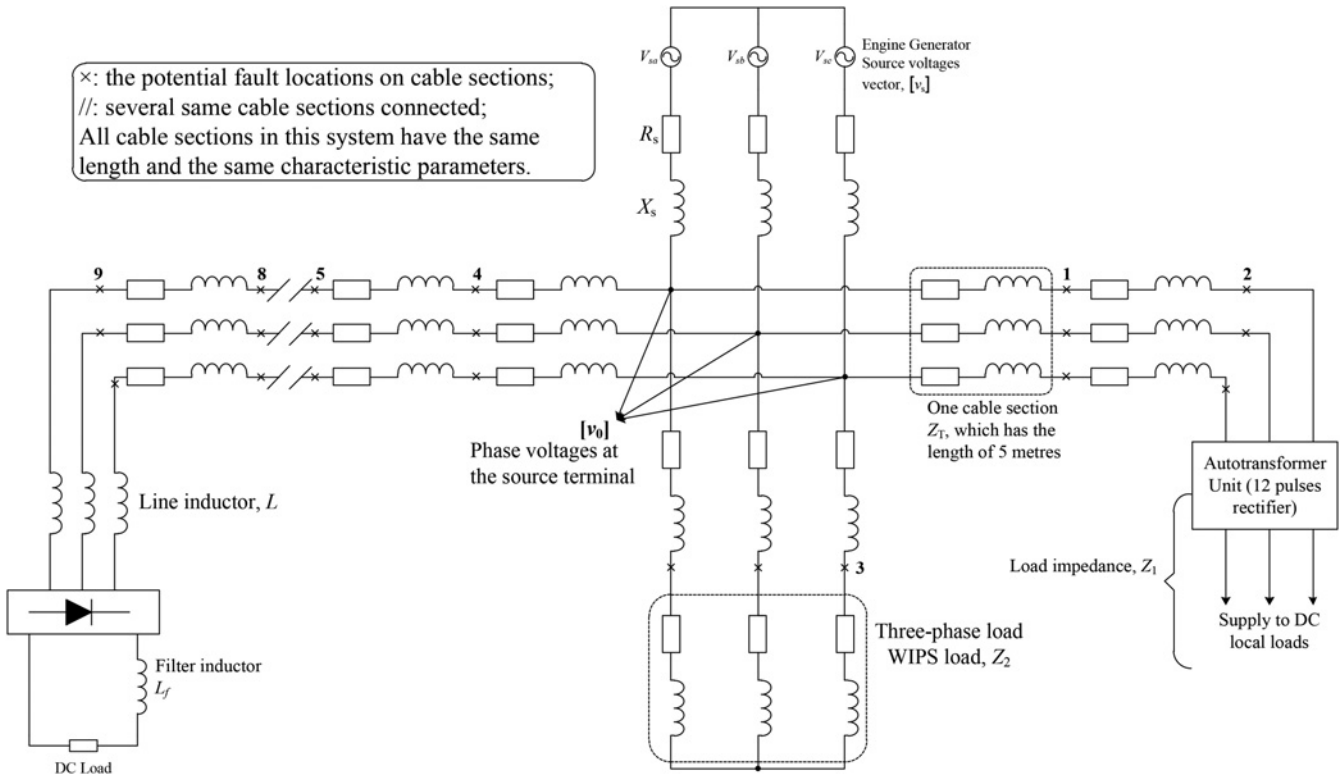

Fig. 1 *Proposed power system for MEA*

doi: 10.1049/iet-est.2011.0056

The third harmonic current amplitude is a function of fault resistance and fault location as will be analysed in this work. Third harmonic currents may be present in a healthy, unbalanced system. However, their amplitude will significantly increase in the presence of an asymmetric fault. Fig. 2 illustrates how the currents to the EMA load change dependent on fault resistances if a fault occurs at fault location 5. Fig. 3 illustrates how the currents to the EMA load change dependent on fault locations if a fault occurs at different fault locations but with the same fault resistance. In both cases, the fault occurred at the time $t = 0.3$ s and Figs. 2 and 3 only recorded currents after the faults occurred. These two examples demonstrate that the harmonic currents are a function of both fault resistance and fault location.

3 Mathematical analysis of the line–line self-impedance at the third harmonic frequency

In the proposed power system, the EMA load is a non-linear load with a line inductance, which distorts the line currents and phase voltages. In this paper, the rectifier switching functions are applied to analyse the harmonic currents produced under unbalanced power supply conditions, which has resulted from an asymmetrical fault occurring in the system (i.e. a phase–phase short-circuit fault through a resistor). Different fault locations and different fault resistances result in different degree of unbalanced phase voltages, which will distort line currents differently. Therefore third harmonic currents will be different and can be proposed for the analysis of fault location and fault resistance.

3.1 Fundamental phase voltages under fault conditions

In this subsection, all variables are referred to the fundamental frequency.

During a fault, the unbalanced phase voltages at the source terminal are dependent on the fault resistance and the fault location. Analysis is based on the phasor algorithm. As shown in Fig. 1, the phase voltages at the source terminal are denoted as a phasor vector $[\boldsymbol{v_0}]$. The engine generator is assumed to generate pure balanced sinusoidal voltages $[v_s]$. At any time, the currents out of the source terminal is equal to the sum of the currents to each load and any abnormal current, for example, fault current, at the fundamental frequency as described in (1)

$$[\boldsymbol{i}] = [i_1] + [i_2] + [i_3] + [i_f] \tag{1}$$

where $[\boldsymbol{i}]$ is the three-phase current phasor vector and represents the source current; $[i_1]$ is the current phasor vector to Load 1; $[i_2]$ is the current to Load 2; $[i_3]$ is the current to Load 3; $[i_f]$ is the fault current flowing to the three-phase system. In this paper, an asymmetrical fault is studied, a phase–phase short-circuit fault with a fault resistance R_f. The three-phase admittance matrix of the fault resistance is denoted as $\boldsymbol{Y}_f$. $[\boldsymbol{v}_f]$ is a phasor vector of

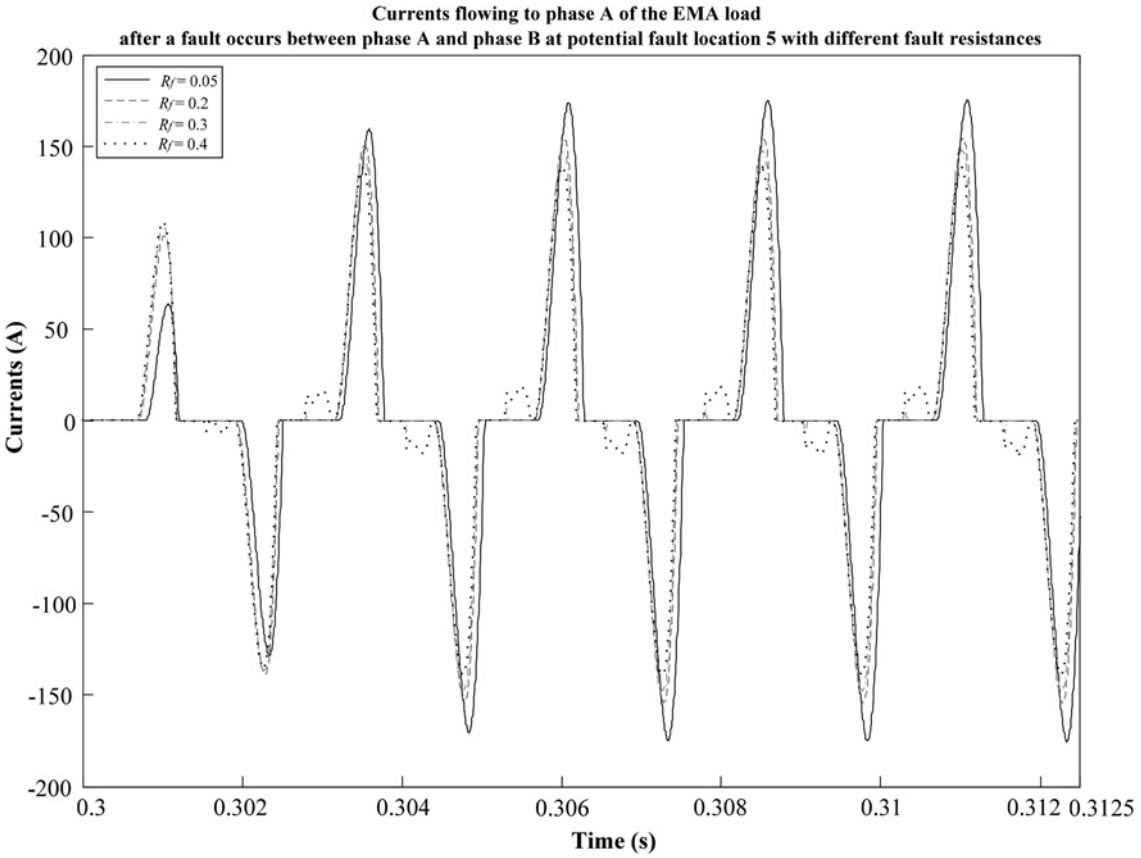

Fig. 2 *Currents flowing to phase A of the EMA load after a fault occurs between phase A and phase B at potential fault location 5 with different fault resistances*

doi: 10.1049/iet-est.2011.0056

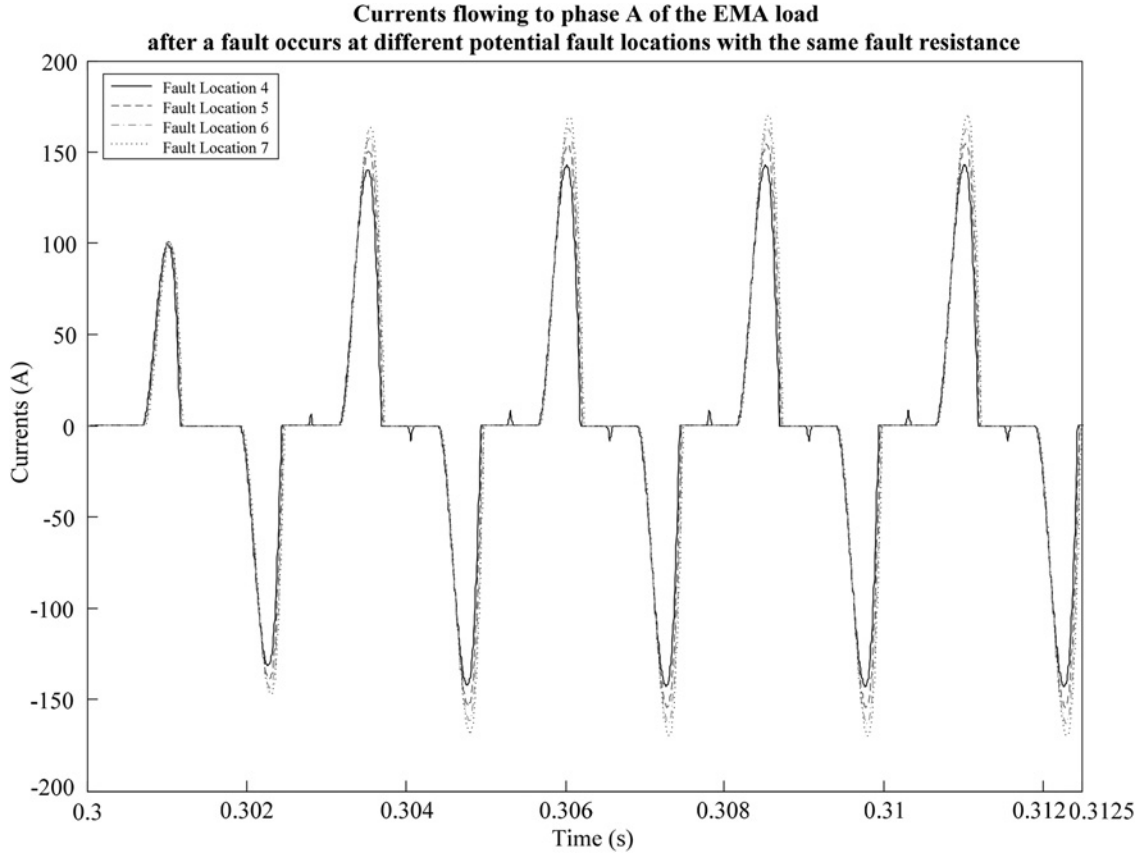

Fig. 3 *Currents flowing to phase A of the EMA load after a fault occurs between phase A and phase B at different potential fault locations with the same fault resistance $R_f = 0.05\ \Omega$*

the phase voltages at the fault location as given in (2).

$$\begin{cases} [i_f] = \boldsymbol{Y}_f\,[\boldsymbol{v}_f] \\ \boldsymbol{Y}_f = \dfrac{1}{R_f}\begin{bmatrix} 1 & -1 & 0 \\ -1 & 1 & 0 \\ 0 & 0 & 0 \end{bmatrix} \end{cases} \tag{2}$$

If a fault occurs on the cable section between Load 1 and the source terminal, the phase voltages at the source terminal are derived as in (3)

$$[\boldsymbol{v}_0] = \left\{I + [\boldsymbol{Z}_s]([\boldsymbol{Y}'_2] + [\boldsymbol{Y}'_3] + [\boldsymbol{Z}_{1f0}]^{-1}\,(I - A))\right\}^{-1}[v_s] \tag{3}$$

where $A = \{I + \boldsymbol{Z}_{1f0}(\boldsymbol{Z}_{1f1} + \boldsymbol{Z}_1)^{-1} + \boldsymbol{Z}_{1f0}\boldsymbol{Y}_f\}^{-1}$; $\boldsymbol{Z}_s$ is the three-phase impedance matrix of the source internal impedance; $\boldsymbol{Y}'_2$ is the three-phase admittance matrix describing admittance of cable connected between the source terminal and Load 2 and admittance of Load 2; and $\boldsymbol{Y}'_3$ is the three-phase admittance matrix describing admittance of cable connected between the source terminal and Load 3 and admittance of Load 3. The detailed expressions for $\boldsymbol{Y}'_2$ and $\boldsymbol{Y}'_3$ are presented in the Appendix. $\boldsymbol{Z}_{1f0}$ is the three-phase impedance matrix of the cables from the fault location to the source terminal; $\boldsymbol{Z}_{1f1}$ is the three-phase impedance matrix of the cables from fault location to Load 1; and $\boldsymbol{Z}_1$ is the three-phase impedance matrix of Load 1.

If a fault occurs on the cable section between the Load 2 and the source terminal, the phase voltages at the source terminal are derived as in (4) in a similar way

$$[\boldsymbol{v}_0] = \left\{I + [\boldsymbol{Z}_s]([\boldsymbol{Y}'_1] + [\boldsymbol{Y}'_3] + [\boldsymbol{Z}_{2f0}]^{-1}\,(I - A))\right\}^{-1}[v_s] \tag{4}$$

where $A = \{I + \boldsymbol{Z}_{2f0}(\boldsymbol{Z}_{2f2} + \boldsymbol{Z}_2)^{-1} + \boldsymbol{Z}_{2f0}Y_f\}^{-1}$; $\boldsymbol{Z}_{2f0}$ is the three-phase impedance matrix of the cables from the fault location to the source terminal; $\boldsymbol{Z}_{2f2}$ is the three-phase impedance matrix of the cables from the fault location to Load 2; and $\boldsymbol{Z}_2$ is the three-phase impedance matrix of Load 2.

If a fault occurs on the cable section between Load 3 and the source terminal, the phase voltages at the source terminal and the phase voltages at the fault location can be calculated as in (5)

$$[\boldsymbol{v}_0] = \left\{I + [\boldsymbol{Z}_s]([\boldsymbol{Y}'_1] + [\boldsymbol{Y}'_2] + [\boldsymbol{Z}_{3f0}]^{-1}\,(I - A))\right\}^{-1}[v_s] \tag{5}$$

3.2 Harmonic AC currents under fault conditions

In the previous subsection, the phase voltages at the source terminal at the fundamental frequency were calculated and can generally be expressed in the time domain as in (6)

$$\begin{cases} v_{a0} = V_{am}\sin(\omega t - \phi_1) \\ v_{b0} = V_{bm}\sin(\omega t - \phi_2) \\ v_{c0} = V_{cm}\sin(\omega t - \phi_3) \end{cases} \tag{6}$$

where v_{a0}, v_{b0} and v_{c0} are instantaneous values of the phase

doi: 10.1049/iet-est.2011.0056

voltages at the source terminal after an asymmetrical fault occurs on a cable section within the system. ϕ_1, ϕ_2 and ϕ_3 are the initial phase angles of the phase voltages at the source terminal with reference to the source supply voltage. Here, it is worth noting that the phase voltages at the source terminal may no longer represent a balanced set of voltages after a fault occurs within the system. The three-phase uncontrolled diode bridge rectifier is as shown in Fig. 4.

v_{a0}, v_{b0} and v_{c0} are the phase voltages at the source terminal. L_a, L_b and L_c are the line inductance including the cable inductances from the source terminal or the fault location to the input terminal of the diode rectifier unit.

The harmonic line currents generated by the diode rectifier are the focus of this work, especially for the third harmonic component. The calculation can be carried out using a Fourier series method and the rectifier switching functions [17–19].

The open-circuit DC output voltage can be derived using voltage rectifier switching functions. The DC output voltage is composed of a smoothed average DC voltage and harmonic components, which produce corresponding DC currents. The harmonic components of the DC voltage and current can be analysed using a combined method proposed in [19]. For accuracy, overlap angles are considered because of the finite inductance connected to the rectifier unit. To simplify the calculation of the AC line currents, it is assumed that the DC current is continuous and smooth.

3.2.1 DC voltage: The DC side voltage v_d is expressed as the sum of the multiplication of the voltage rectifier switching functions S_a, S_b and S_c and the relative phase voltages v_{a0}, v_{b0} and v_{c0}.

$$v_d = S_a\, v_{a0} + S_b\, v_{b0} + S_c\, v_{c0} \tag{7}$$

The voltage rectifier switching functions are as shown in Fig. 5. These rectifier switching functions can be expressed as a Fourier series as follows

$$\begin{cases} S_a = \sum\limits_{n=1,3,5,\ldots}^{\infty} \left(A_{an}\cos n\omega t + B_{an}\sin n\omega t\right) \\ S_b = \sum\limits_{n=1,3,5,\ldots}^{\infty} \left(A_{bn}\cos n\omega t + B_{bn}\sin n\omega t\right) \\ S_c = \sum\limits_{n=1,3,5,\ldots}^{\infty} \left(A_{cn}\cos n\omega t + B_{cn}\sin n\omega t\right) \end{cases} \tag{8}$$

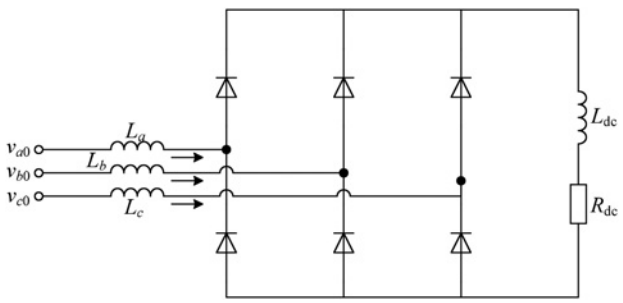

Fig. 4 *Three-phase uncontrolled diode rectifier bridge unit (EMA load, Load 3)*

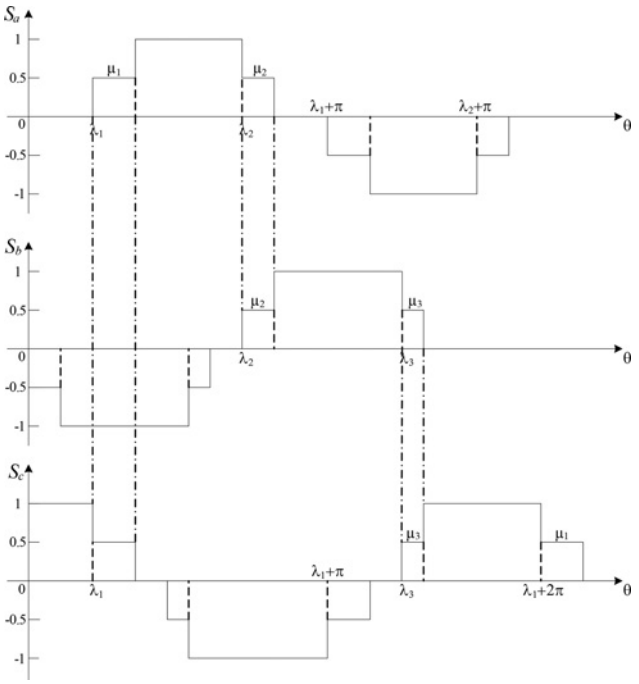

Fig. 5 *Rectifier switching functions for calculating the DC output voltage*

Here

$$A_{an} = \frac{-2}{n\pi}\left\{\sin n\left(\lambda_1+\frac{\mu_1}{2}\right)\cos\left(\frac{n\mu_1}{2}\right) - \sin n\left(\lambda_2+\frac{\mu_2}{2}\right)\cos\left(\frac{n\mu_2}{2}\right)\right\}$$

$$B_{an} = \frac{2}{n\pi}\left\{\cos n\left(\lambda_1+\frac{\mu_1}{2}\right)\cos\left(\frac{n\mu_1}{2}\right) - \cos n\left(\lambda_2+\frac{\mu_2}{2}\right)\cos\left(\frac{n\mu_2}{2}\right)\right\}$$

$$A_{bn} = \frac{-2}{n\pi}\left\{\sin n\left(\lambda_2+\frac{\mu_2}{2}\right)\cos\left(\frac{n\mu_2}{2}\right) - \sin n\left(\lambda_3+\frac{\mu_3}{2}\right)\cos\left(\frac{n\mu_3}{2}\right)\right\}$$

$$B_{bn} = \frac{2}{n\pi}\left\{\cos n\left(\lambda_2+\frac{\mu_2}{2}\right)\cos\left(\frac{n\mu_2}{2}\right) - \cos n\left(\lambda_3+\frac{\mu_3}{2}\right)\cos\left(\frac{n\mu_3}{2}\right)\right\}$$

$$A_{cn} = \frac{-2}{n\pi}\left\{\sin n\left(\lambda_3+\frac{\mu_3}{2}\right)\cos\left(\frac{n\mu_3}{2}\right) - \sin n\left(\lambda_1+\frac{\mu_1}{2}\right)\cos\left(\frac{n\mu_1}{2}\right)\right\}$$

$$B_{cn} = \frac{2}{n\pi}\left\{\cos n\left(\lambda_3+\frac{\mu_3}{2}\right)\cos\left(\frac{n\mu_3}{2}\right) - \cos n\left(\lambda_1+\frac{\mu_1}{2}\right)\cos\left(\frac{n\mu_1}{2}\right)\right\}$$

μ_1, μ_2 and μ_3 are the overlap angles of the respective phases,

doi: 10.1049/iet-est.2011.0056

as shown in Fig. 5. The overlap angles are calculated by

$$\begin{cases} \mu_1 = \cos^{-1}\left\{1 - \dfrac{(X_a + X_c)I_d}{\sqrt{V_{cm}^2 + V_{am}^2 - 2V_{am}V_{cm}\cos(\phi_3 - \phi_1)}}\right\} \\ \mu_2 = \cos^{-1}\left\{1 - \dfrac{(X_a + X_b)I_d}{\sqrt{V_{bm}^2 + V_{am}^2 - 2V_{am}V_{bm}\cos(\phi_1 - \phi_2)}}\right\} \\ \mu_3 = \cos^{-1}\left\{1 - \dfrac{(X_c + X_b)I_d}{\sqrt{V_{cm}^2 + V_{bm}^2 - 2V_{bm}V_{cm}\cos(\phi_2 - \phi_3)}}\right\} \end{cases}$$

λ_1, λ_2 and λ_3 are the radian phase angles at which the phase voltages at the corresponding phases are equal to each other and have positive values. They are calculated as

$$\lambda_1 = \tan^{-1}\frac{-V_{cm}\sin\phi_3 + V_{am}\sin\phi_1}{-V_{cm}\cos\phi_3 + V_{am}\cos\phi_1}$$

$$\lambda_2 = \tan^{-1}\frac{-V_{am}\sin\phi_1 + V_{bm}\sin\phi_2}{-V_{am}\cos\phi_1 + V_{bm}\cos\phi_2}$$

$$\lambda_3 = \tan^{-1}\frac{-V_{bm}\sin\phi_2 + V_{cm}\sin\phi_3}{-V_{bm}\cos\phi_2 + V_{cm}\cos\phi_3}$$

Substituting (6) and (8) into (7), the DC voltage is given as

$$v_d = V_{d0} + \sum_{n=2,4,6,\ldots}^{\infty}\left(A_{dn}\cos n\,\omega t + B_{dn}\sin n\,\omega t\right) \quad (9)$$

Here

$$V_{d0} = \frac{1}{2}\left[V_{am}\left(-A_{a1}\sin\varphi_1 + B_{a1}\cos\varphi_1\right) + V_{bm}\left(-A_{b1}\sin\varphi_2 + B_{b1}\cos\varphi_2\right) + V_{cm}\left(-A_{c1}\sin\varphi_3 + B_{c1}\cos\varphi_3\right)\right]$$

(see (10))

The first term on the right-hand side of (9) represents the DC component of the voltage on the DC side and the remaining terms are the harmonic components. With the DC voltage defined, the DC current can be derived.

3.2.2 DC current: The DC current can be determined by applying the DC side voltage and the load impedances at the corresponding harmonic frequencies. For the kth harmonic, the load impedance is $Z_k = R_{dc} + jkX_{dc}$. The DC current is expressed as

$$i_d = I_{d0} + \sum_{k=2,4,6,\ldots}^{\infty} I_{dk}\cos\left(k\omega t - \beta_k\right) \quad (11)$$

Here

$$I_d = V_{d0}/R_{dc}, \quad I_{dk} = \frac{\sqrt{A_{dk}^2 + B_{dk}^2}}{|Z_k|} \quad (11)$$

A_{dk} and B_{dk} are given by (10)

$$\beta_k = \tan^{-1}\frac{B_{dk}}{A_{dk}} + \tan^{-1}\frac{\mathrm{Im}(Z_k)}{\mathrm{Re}(Z_k)}$$

3.2.3 AC current: The AC line currents are produced by the DC current i_d. The AC line currents can be derived by multiplying the DC current with the current rectifier switching functions. Owing to the finite line inductance, the commutation of diodes between phases exists and the assumption here is that, during the commutation period, the DC current is constant. This simplifies the analysis. The change of the line current is assumed to be linear. The current rectifier switching function for phase A is as shown in Fig. 6.

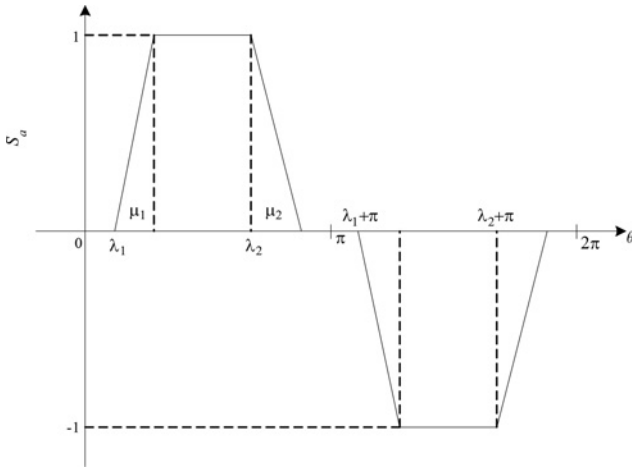

Fig. 6 *Rectifier switching function for calculating AC line currents*

$$\begin{cases} A_{dn} = (-1/2)\left\{V_{am}\left[\left(A_{a(n-1)} + A_{a(n+1)}\right)\sin\varphi_1 + \left(B_{a(n-1)} - B_{a(n+1)}\right)\cos\varphi_1\right]\right. \\ \qquad +V_{bm}\left[\left(A_{a(n-1)} + A_{a(n+1)}\right)\sin\varphi_2 + \left(B_{a(n-1)} - B_{a(n+1)}\right)\cos\varphi_2\right] \\ \qquad \left.+V_{cm}\left[\left(A_{a(n-1)} + A_{a(n+1)}\right)\sin\varphi_3 + \left(B_{a(n-1)} - B_{a(n+1)}\right)\cos\varphi_3\right]\right\} \\ B_{dn} = (+1/2)\left\{V_{am}\left[\left(A_{a(n-1)} - A_{a(n+1)}\right)\cos\varphi_1 - \left(B_{a(n-1)} + B_{a(n+1)}\right)\sin\varphi_1\right]\right. \\ \qquad +V_{bm}\left[\left(A_{a(n-1)} - A_{a(n+1)}\right)\cos\varphi_2 - \left(B_{a(n-1)} + B_{a(n+1)}\right)\sin\varphi_2\right] \\ \qquad \left.+V_{cm}\left[\left(A_{a(n-1)} - A_{a(n+1)}\right)\cos\varphi_3 - \left(B_{a(n-1)} + B_{a(n+1)}\right)\sin\varphi_3\right]\right\} \end{cases} \quad (10)$$

$$n = 2m \quad (m = 1, 2, 3\ldots)$$

doi: 10.1049/iet-est.2011.0056

The current rectifier switching function can be expressed by a Fourier series as

$$S_{ia}(t) = \sum_{n=1,3,5,\ldots}^{\infty} A_{ian}\cos n\,\omega t + B_{ian}\sin n\,\omega t \tag{12}$$

Here

$$A_{ian} = \frac{4}{n^2\pi}\left\{\frac{-1}{\mu_1}\sin\frac{n\mu_1}{2}\sin n\left(\lambda_1+\frac{\mu_1}{2}\right)+\frac{1}{\mu_2}\sin\frac{n\mu_2}{2}\sin n\left(\lambda_2+\frac{\mu_2}{2}\right)\right\}$$

$$B_{ian} = \frac{4}{n^2\pi}\left\{\frac{1}{\mu_1}\sin\frac{n\mu_1}{2}\cos n\left(\lambda_1+\frac{\mu_1}{2}\right)-\frac{1}{\mu_2}\sin\frac{n\mu_2}{2}\cos n\left(\lambda_2+\frac{\mu_2}{2}\right)\right\}$$

The third harmonic is used in this work. Therefore the third harmonic AC line current on phase A is derived by multiplication of the switching function with the DC current and given as

$$\begin{aligned} i_{a3} &= I_{d0}\sqrt{A_{ia3}^2+B_{ia3}^2}\cos(3\omega t-\varphi_3) \\ &\quad + I_{d2}\frac{\sqrt{A_{ia1}^2+B_{ia1}^2}}{2}\cos(3\omega t-\beta_3-\varphi_1)+\cdots \\ &\quad \times\sum_{l=1,2,3,\ldots}^{\infty} I_{d(2l)}\frac{\sqrt{A_{ia(2l+3)}^2+B_{ia(2l+3)}^2}}{2} \\ &\quad \cos\left(3\omega t+\beta_{(2l)}+\varphi_{(2l+3)}\right)+\cdots \\ &\quad \times\sum_{l=2,3,4,\ldots}^{\infty} I_{d(2l)}\frac{\sqrt{A_{ia(2l-3)}^2+B_{ia(2l-3)}^2}}{2} \\ &\quad \cos\left(3\omega t-\beta_{(2l)}-\varphi_{(2l-3)}\right) \end{aligned} \tag{13}$$

Here

$$\varphi_{(2l+3)} = \tan^{-1}\frac{B_{ia(2l+3)}}{A_{ia(2l+3)}} \quad\text{and}\quad \varphi_{(2l-3)} = \tan^{-1}\frac{B_{ia(2l-3)}}{A_{ia(2l-3)}}$$

In a similar way, the third harmonic AC line currents on phases B and C can be calculated.

In the proposed simplified aircraft power system, the uncontrolled diode bridge rectifier unit is the only non-linear load, which is also the third harmonic current source when it is applied under unbalanced supply condition (e.g. an asymmetrical phase–phase fault). The third harmonic voltage distortions at each node or load terminal can be calculated using the topological circuit of the system with parameters at the third harmonic frequency and will be discussed in the follow subsection.

3.3 Third harmonic line currents at each load

In this subsection, the third harmonic line currents flowing to each load will be discussed and derived. The supply is assumed to generate a pure sinusoidal voltage at the fundamental frequency. Therefore the Thevenin equivalent of the supply will be short-circuited when a topological circuit at the harmonic frequencies is considered. All impedance values, voltages and currents vectors are referred to the third harmonic frequency.

In an analogous way as described in the previous subsection, the third harmonic line currents flowing to each load can be derived and calculated. The third harmonic currents produced are circulated within the system and can be expressed by the sum of the load currents (including the source current) and fault currents at the third harmonic frequency

$$[i_3]_{3f_0} = [i_s]_{3f_0} + [i_1]_{3f_0} + [i_2]_{3f_0} + [i_f]_{3f_0} \tag{14}$$

Here $[i_1]_{3f_0}$, $[i_2]_{3f_0}$ and $[i_3]_{3f_0}$ are the third harmonic AC line currents flowing to each load; $[i_s]_{3f_0}$ is the third harmonic line current flowing to the source from the non-linear load; $[i_f]_{3f_0}$ is the fault current at the third harmonic frequency. The third harmonic line currents are dependent on where the fault location is. In the following description within this subsection, all variables are referred to the third harmonic frequency and the subscripts $3f_0$ are omitted.

3.3.1 Fault occurring on cables supplying Load 1:

For a fault on the cable section supplying Load 1, the phase voltages at the source terminal at the third harmonic frequency are expressed by

$$[\boldsymbol{v}_0] = \left\{Y_s + Y_2//Y_{T2} + Y_{1f0}(I-A)\right\}^{-1}[i_3] \tag{15}$$

Here $A = \{I + Z_{1f0}(Z_{1f1}+Z_1)^{-1} + Z_{1f0}\boldsymbol{Y}_f\}^{-1}$. Then, the third harmonic currents flowing to Load 1 and Load 2 can be calculated as

$$\begin{cases} [i_1] = \{Y_{1f0} - (Y_{1f0}+Y_f)A\}[v_0] \\ [i_2] = (Z_2+Z_{T2})^{-1}[v_0] \end{cases} \tag{16}$$

The third harmonic phase voltages at the Load 3 are expressed as

$$[v_3] = \left\{I + Z_{T3}(Y_s + Y_2//Y_{T2} + Y_{1f0}(I-A))\right\}[v_0] \tag{17}$$

3.3.2 Fault occurring on cables supplying Load 2:

Similarly, for a fault on the cable section supplying Load 2, the phase voltages at the source terminal at the third harmonic frequency are calculated by

$$[\boldsymbol{v}_0] = \left\{Y_s + Y_1//Y_{T1} + Y_{2f0}(I-A)\right\}^{-1}[i_3] \tag{18}$$

Here $A = \{I + Z_{2f0}(Z_{2f2}+Z_2)^{-1} + Z_{2f0}Y_f\}^{-1}$. The third harmonic currents flowing to Load 1 and Load 2 are expressed as

$$\begin{cases} [i_1] = \left(Z_1+Z_{T1}\right)^{-1}[\boldsymbol{v}_0] \\ [i_2] = \left\{Y_{2f0} - \left(Y_{2f0}+\boldsymbol{Y}_f\right)A\right\}[\boldsymbol{v}_0] \end{cases} \tag{19}$$

doi: 10.1049/iet-est.2011.0056

The third harmonic phase voltages at the Load 3 are given by

$$[v_3] = \left\{I + Z_{T3}(Y_s + Y_1//Y_{T1} + Y_{2f0}(I - A))\right\}[\boldsymbol{v}_0] \quad (20)$$

3.3.3 Fault occurring on cables supplying Load 3:

The third harmonic phase voltages at the source terminal for a fault on the cable section to Load 3 are calculated as

$$[\boldsymbol{v}_0] = \left\{\boldsymbol{Y}_{\text{eq}} + \boldsymbol{Y}_f\left(I + Y_{3f0}^{-1}\boldsymbol{Y}_{\text{eq}}\right)\right\}^{-1}[i_3] \quad (21)$$

Here, the equivalent admittance matrix $\boldsymbol{Y}_{\text{eq}}$ is defined and expressed as $\boldsymbol{Y}_{\text{eq}} = Y_s + Y_1//Y_{T1} + Y_2//Y_{T2}$. The phase voltages at the Load 3 are calculated as

$$[v_3] = \left\{Y_{3f3}^{-1}\boldsymbol{Y}_{\text{eq}} + \left(Y_{3f3}^{-1}\boldsymbol{Y}_f + I\right)\left(I + Y_{3f0}^{-1}\boldsymbol{Y}_{\text{eq}}\right)\right\}[\boldsymbol{v}_0] \quad (22)$$

The third harmonic currents flowing to the Load 1 and Load 2 are calculated as

$$\begin{cases}[i_1] = \left(Z_1 + Z_{T1}\right)^{-1}[\boldsymbol{v}_0] \\ [i_2] = \left(Z_2 + Z_{T2}\right)^{-1}[\boldsymbol{v}_0]\end{cases} \quad (23)$$

In this section, the third harmonic line currents flowing to or from each load are discussed and analysed. According to the definition of the line–line self-impedance at the harmonic frequency [14], the impedance indicators can be obtained. Here, a different expression of the line–line self-impedance is used. For the proposed aircraft electrical system, three-phase loads are assumed to be balanced and denoted as Z_1, Z_2 and Z_3. Thus, the three line–line self-impedance are given by

$$\begin{cases}Z_{ab1} = Z_1\left(1 - \dfrac{i_1(b)}{i_1(a)}\right) \\ Z_{ab2} = Z_2\left(1 - \dfrac{i_2(b)}{i_2(a)}\right) \\ Z_{ab3} = \dfrac{v_3(a) - v_3(b)}{i_3(a)}\end{cases} \quad (24)$$

In the above definitions, the line–line self-impedance at the non-linear load terminal (3) is defined by voltage and current and cannot be simplified as the other two due to the non-linearities of its load. Here, all impedances are referred to the third harmonic frequency; load line currents and phase voltages at the load terminal are also referred to the third harmonic components and as derived as in Section 3.3.

4 Comparison results

In this section, the comparison of the equivalent line–line self-impedance curves against fault location and fault resistance, which are obtained using the mathematical analysis results and through simulation, will be presented. The fault resistance range studied is from 0.01 up to 0.50

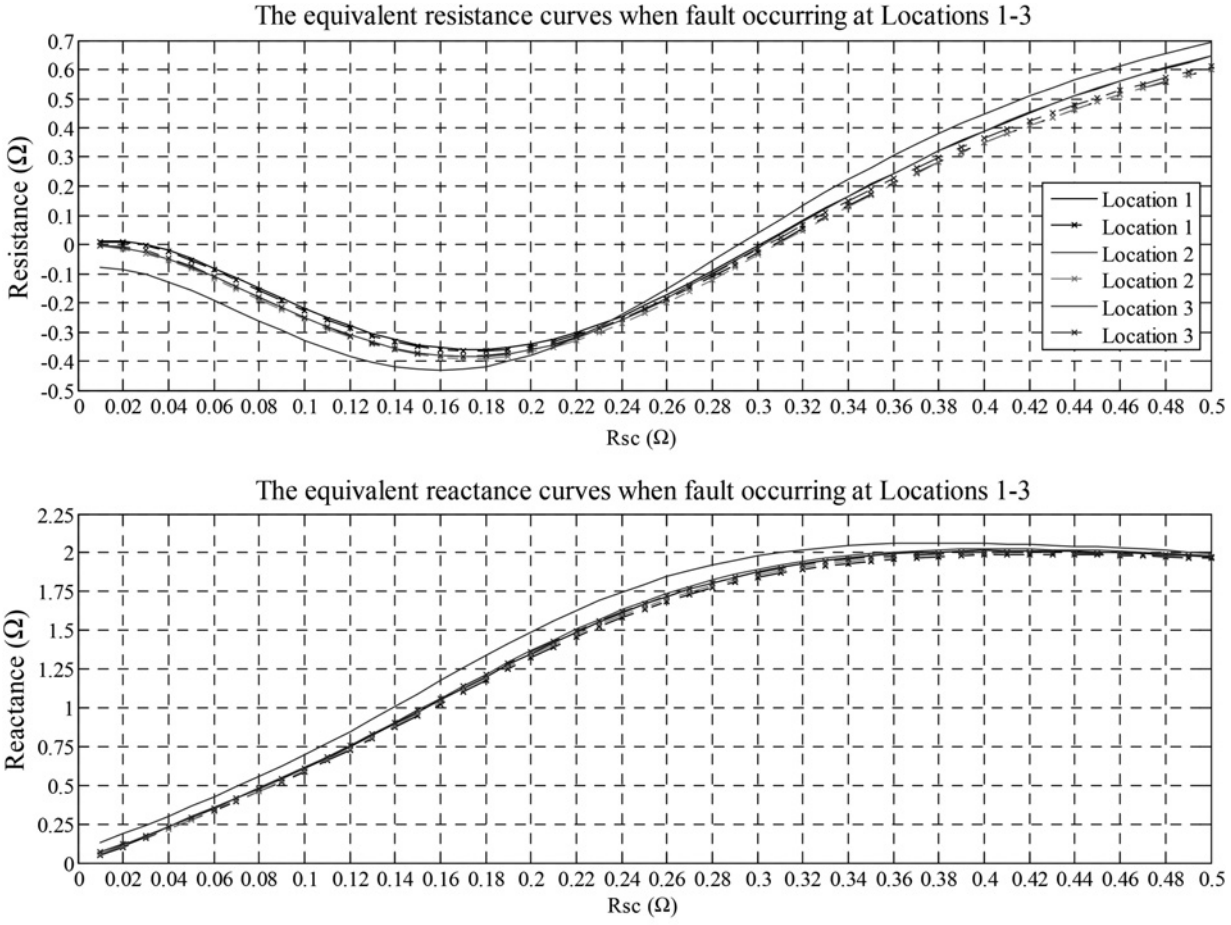

Fig. 7 *Equivalent impedance curves seen from Load 1 when fault occurs at Locations 1–3 (solid line, results from the simulation; dash dot with 'x' line, results from the mathematical analysis)*

doi: 10.1049/iet-est.2011.0056

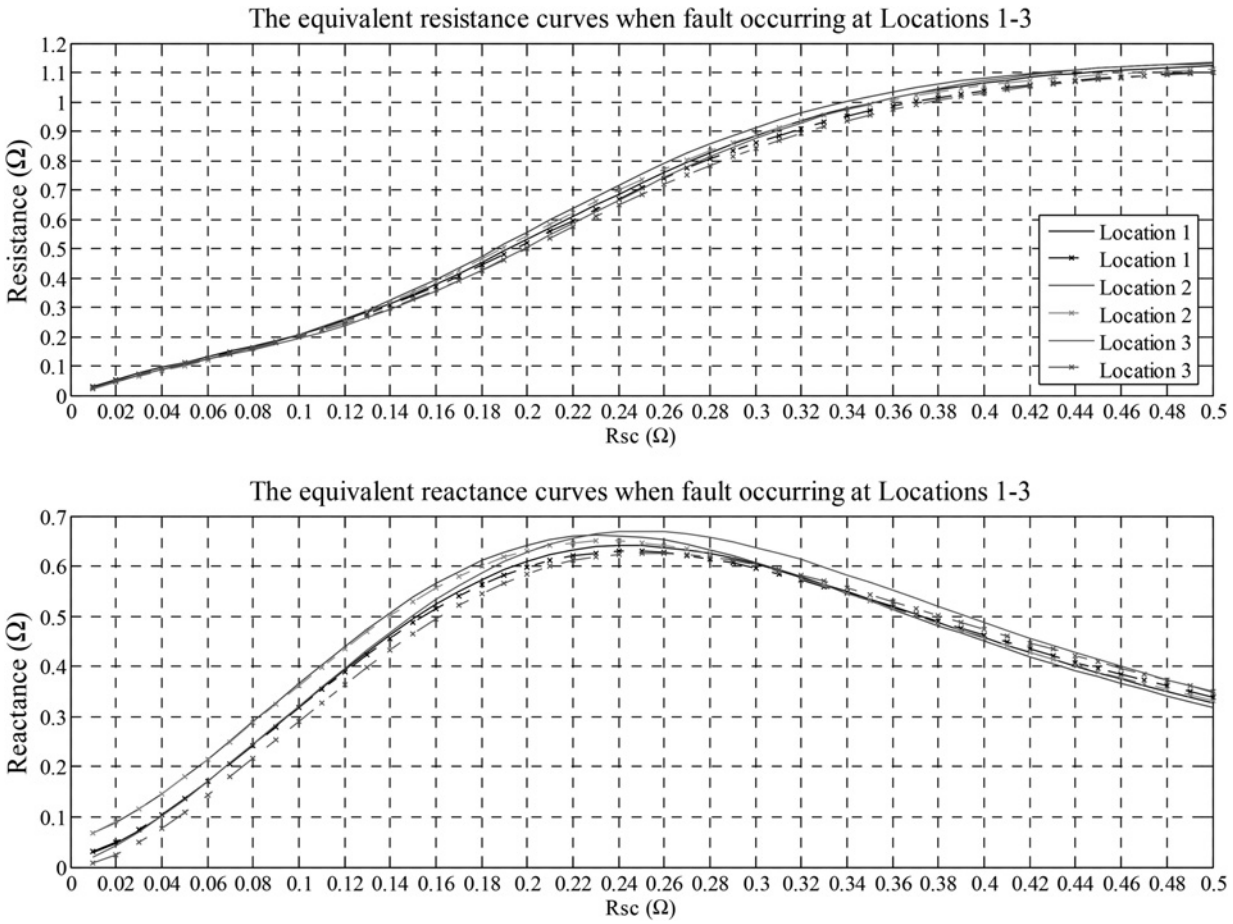

Fig. 8 *Equivalent impedance curves seen from Load 2 when fault occurs at Locations 1–3 (solid line, results from the simulation; dash dot with 'x' line, results from the mathematical analysis)*

Ω. The system was simulated using SIMPOWER block in MATLAB/SIMULINK. The relationship of the equivalent line–line self-impedance curves against fault location and fault resistance was similar to the experimental results presented in [16].

Figs. 7–9 show the observed equivalent impedances measured under fault conditions at each of the load terminals for a range of fault resistance and locations as given by simulation and mathematical analysis. From Fig. 7–9, the equivalent impedance curves obtained by mathematical analysis are similar to those obtained from simulation. These curves for different fault locations at the third harmonic frequency are very close to each other. It will therefore be difficult to distinguish faults if they occur at these locations.

Fig. 10 shows the equivalent impedance curves obtained at Load 1 when fault occurring at Locations 4–6 (solid line, results from the simulation; dash dot with 'x' line, results from the mathematical analysis).

Figs. 10–15 show the equivalent line–line self-impedance (including self-resistance and self-reactance) curves at each load when a fault occurs at locations 4–9 deduced from mathematical analysis and simulation. The mathematical analysis and simulation results are in good agreement. To distinguish the faults on cable Sections 4–9, for low fault resistances up to 0.2 Ω, the equivalent line–line self-impedance at the non-linear load can be used to locate these faults. For high fault resistances, the equivalent line–line self-impedance at the linear loads can be used to locate the faults. This is because of the degree of imbalance decreasing and more information is required to discriminate faults. Thus by using a combination of all the measured impedance it may be possible to locate fault on a long line section [14, 15].

It can be seen that the curves found from the mathematical analysis have similar trends to those from the simulation model. The differences between them are because of the calculation errors of the phase angles and amplitudes of the third harmonic currents produced by the diode bridge rectifier. In this simulation, the length interval of the fault location is 5 m. If the interval is decreased, for the equivalent impedance curves against fault location and fault resistance, the differences between them will be less obvious so that the combination of them may not be able to identify faults occurring at a resolution much less than 5 m.

Mathematical analysis of the line–line self-impedance at the third harmonic frequency was presented in this paper. To apply this algorithm in fault detection, the currents to load need to be continuously monitored and analysed in the frequency domain. If third harmonic currents are detected, the line–line self-impedances at the third harmonic frequency for each load will be calculated using the monitored currents and voltages. Then, the calculated equivalent impedances obtained for each load will be compared with the calibrated curves of equivalent impedances against fault location. Note that the load currents and voltages are continuously monitored so that the load impedances can be continuously updated for use in the algorithm.

doi: 10.1049/iet-est.2011.0056

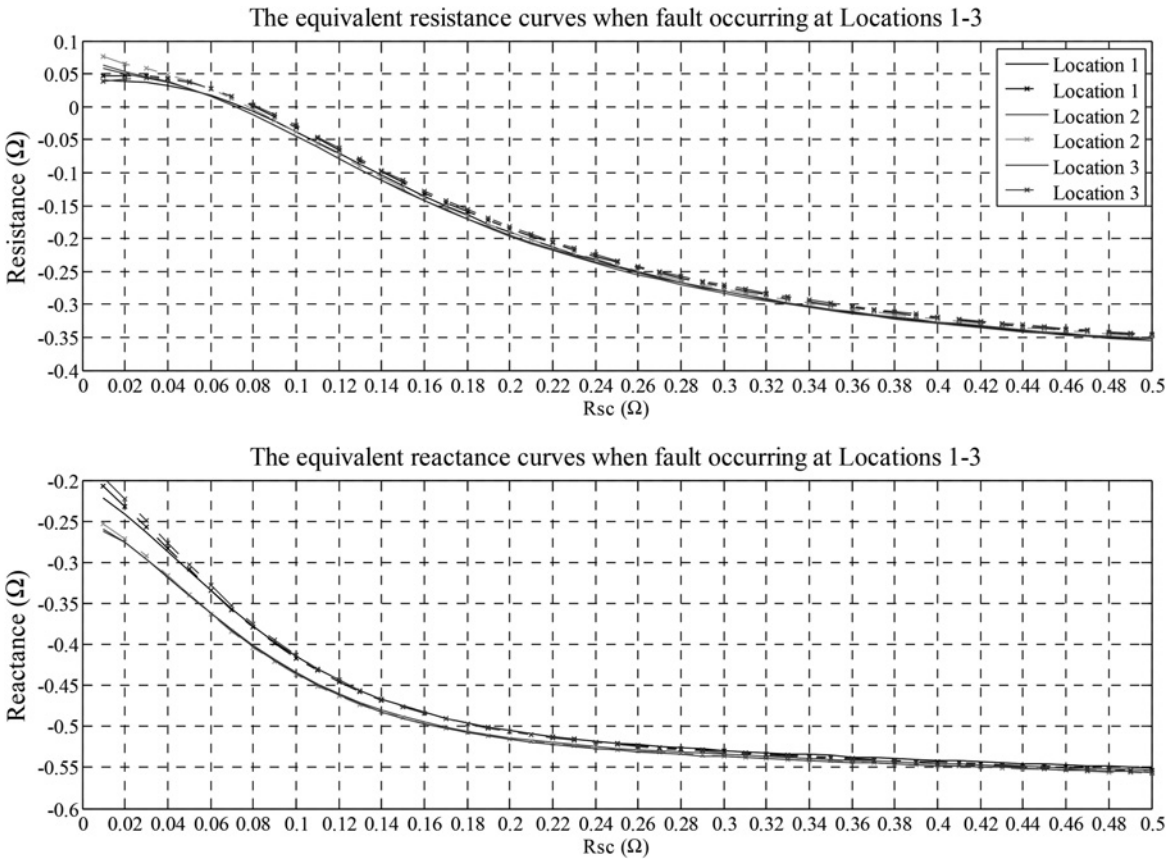

Fig. 9 *Equivalent impedance curves seen from Load 3 when fault occurs at Locations 1–3 (solid line, results from the simulation; dash dot with 'x' line, results from the mathematical analysis)*

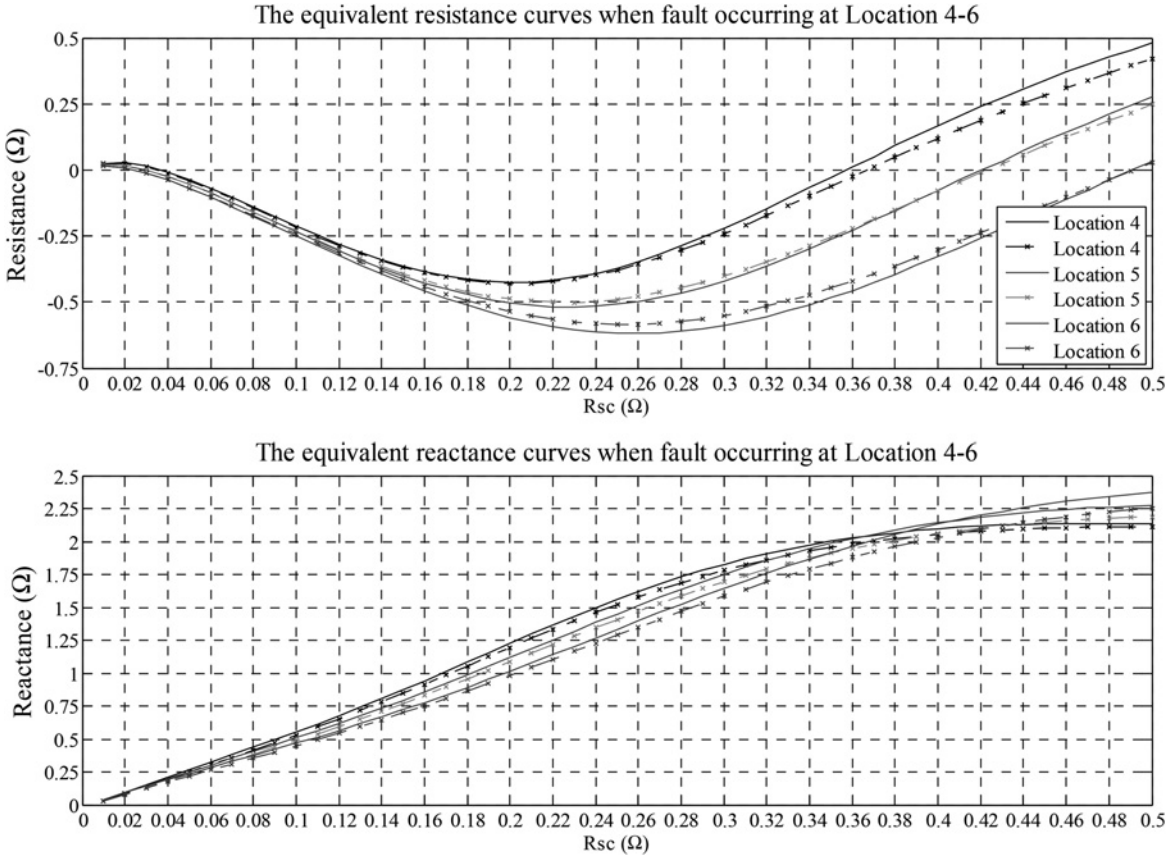

Fig. 10 *The equivalent impedance curves obtained at Load 1 when fault occurring at Locations 4–6 (solid line, results from the simulation; dash dot with 'x' line, results from the mathematical analysis)*

doi: 10.1049/iet-est.2011.0056

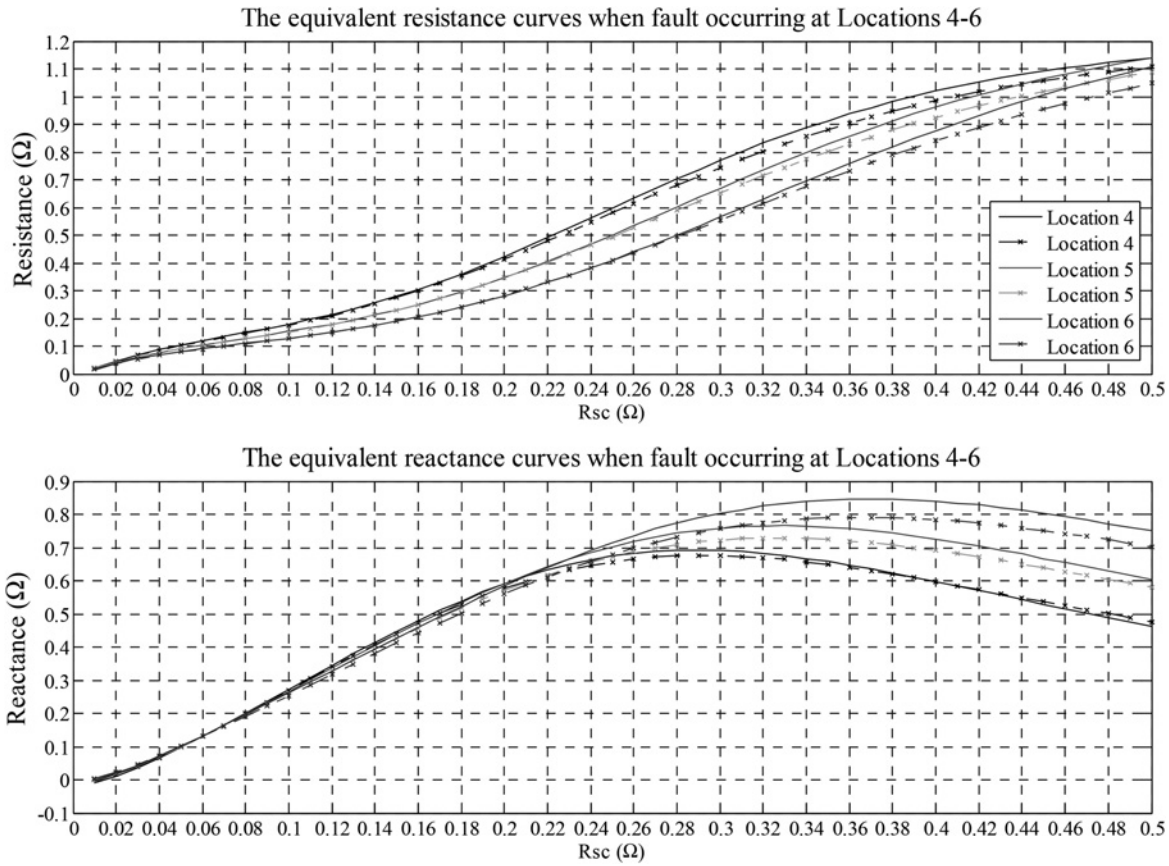

Fig. 11 *Equivalent impedance curves obtained at Load 2 when fault occurring at Locations 4–6 (solid line, results from the simulation; dash dot with 'x' line, results from the mathematical analysis)*

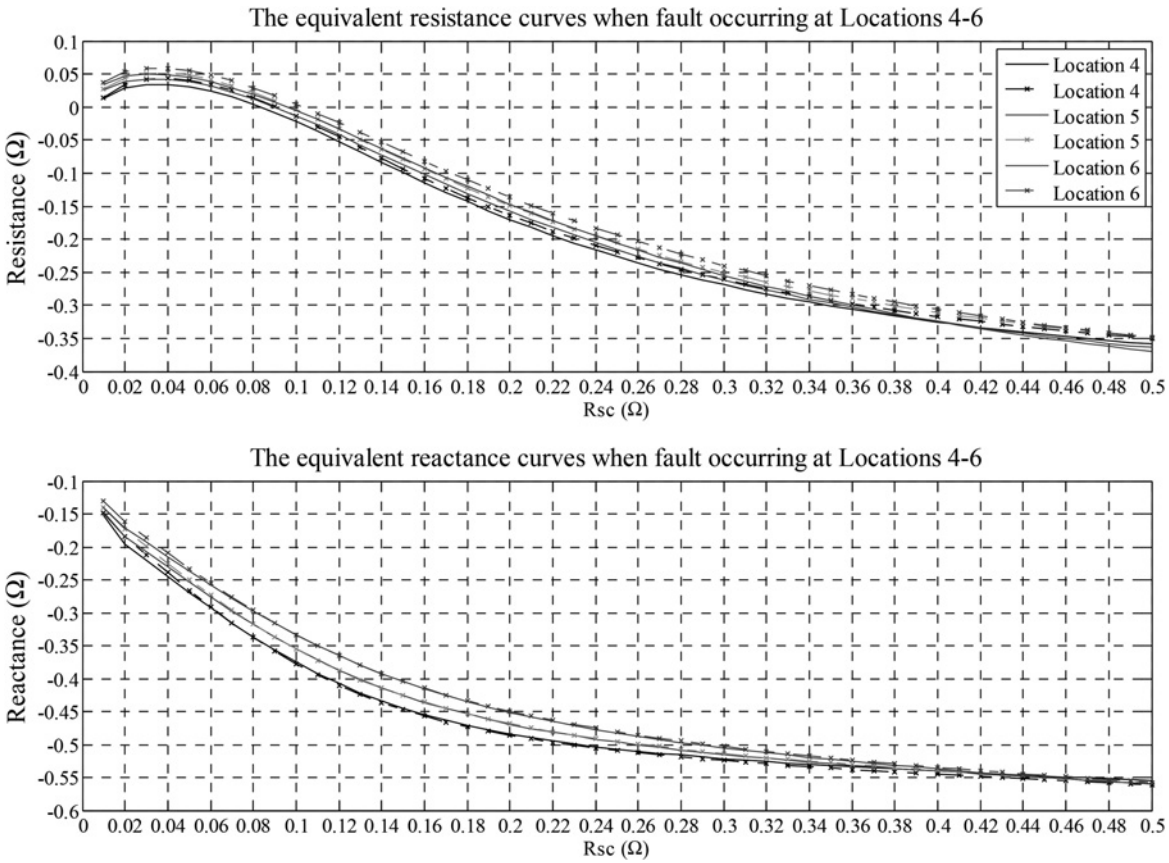

Fig. 12 *Equivalent impedance curves obtained at Load 3 when fault occurring at Locations 4–6 (solid line, results from the simulation; dash dot with 'x' line, results from the mathematical analysis)*

doi: 10.1049/iet-est.2011.0056

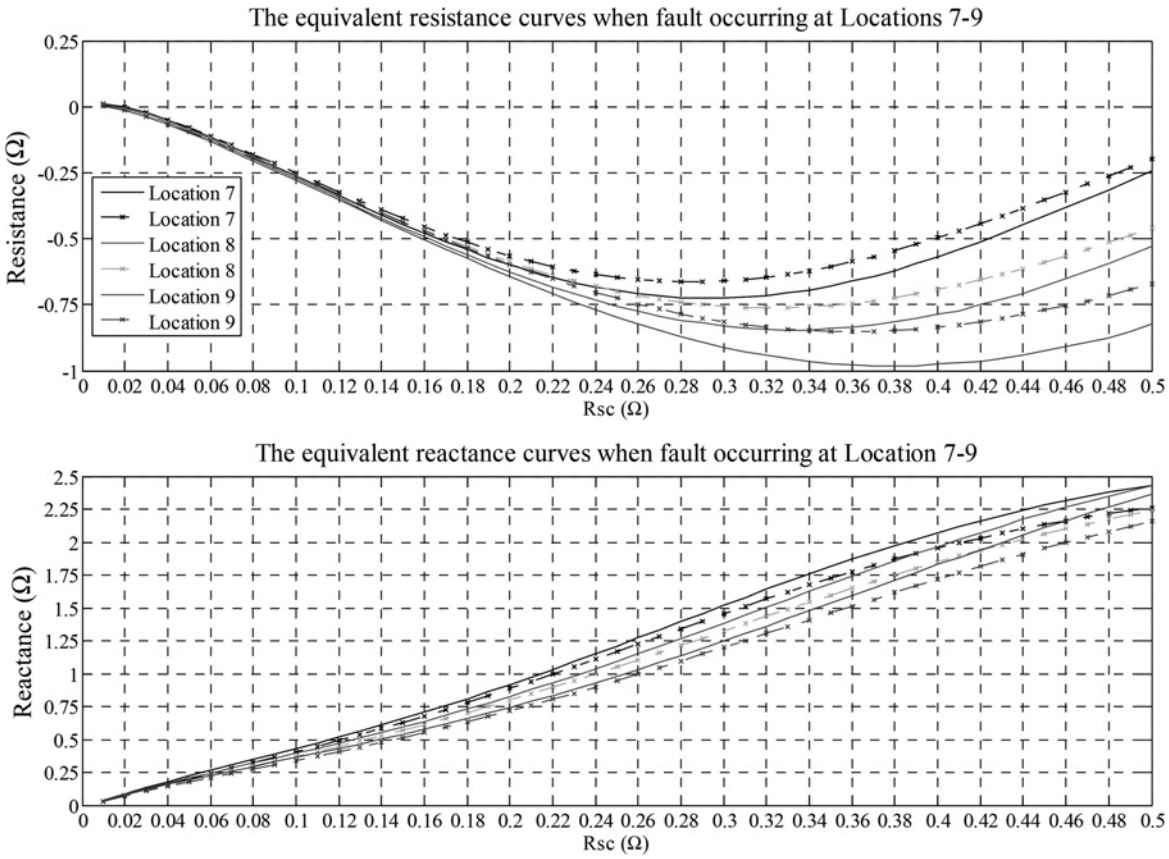

Fig. 13 *Equivalent impedance curves obtained at Load 1 when fault occurring at Locations 7–9 (solid line, results from the simulation; dash dot with 'x' line, results from the mathematical analysis)*

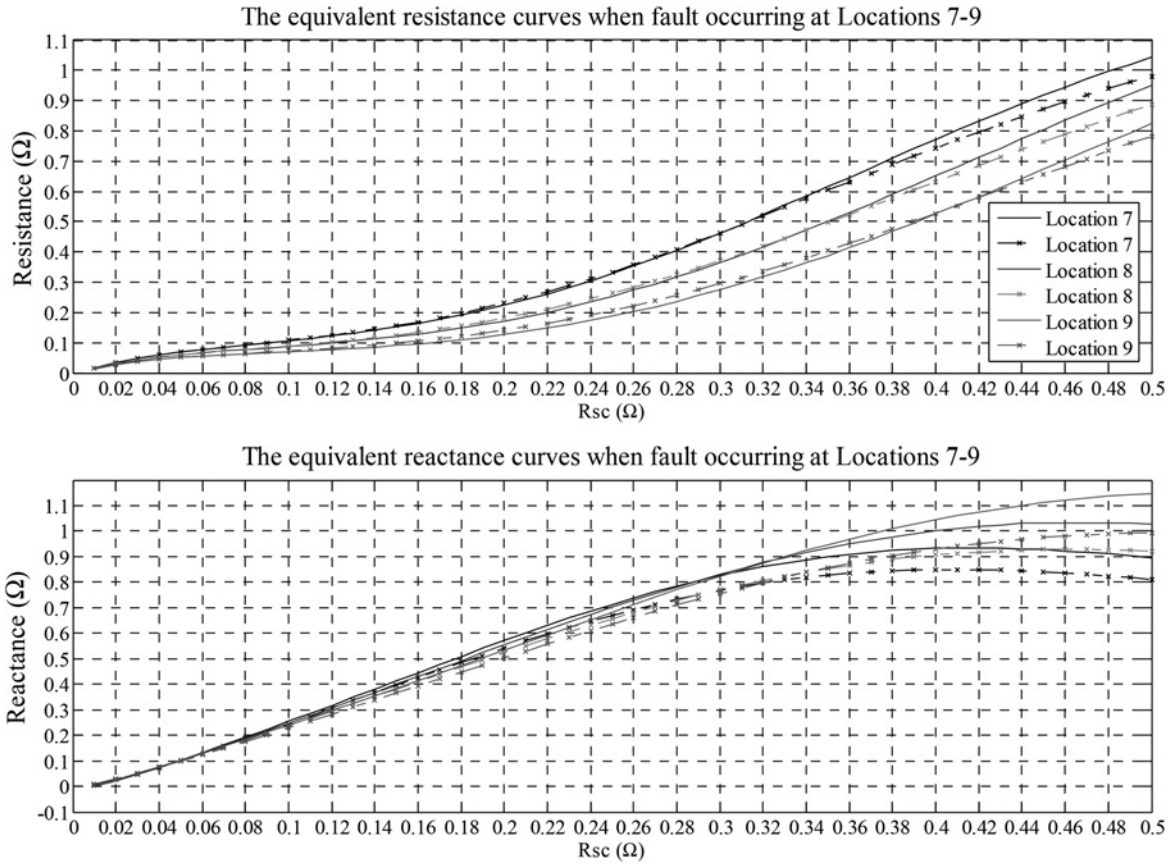

Fig. 14 *Equivalent impedance curves obtained at Load 2 when fault occurring at Locations 7–9 (solid line, results from the simulation; dash dot with 'x' line, results from the mathematical analysis)*

doi: 10.1049/iet-est.2011.0056

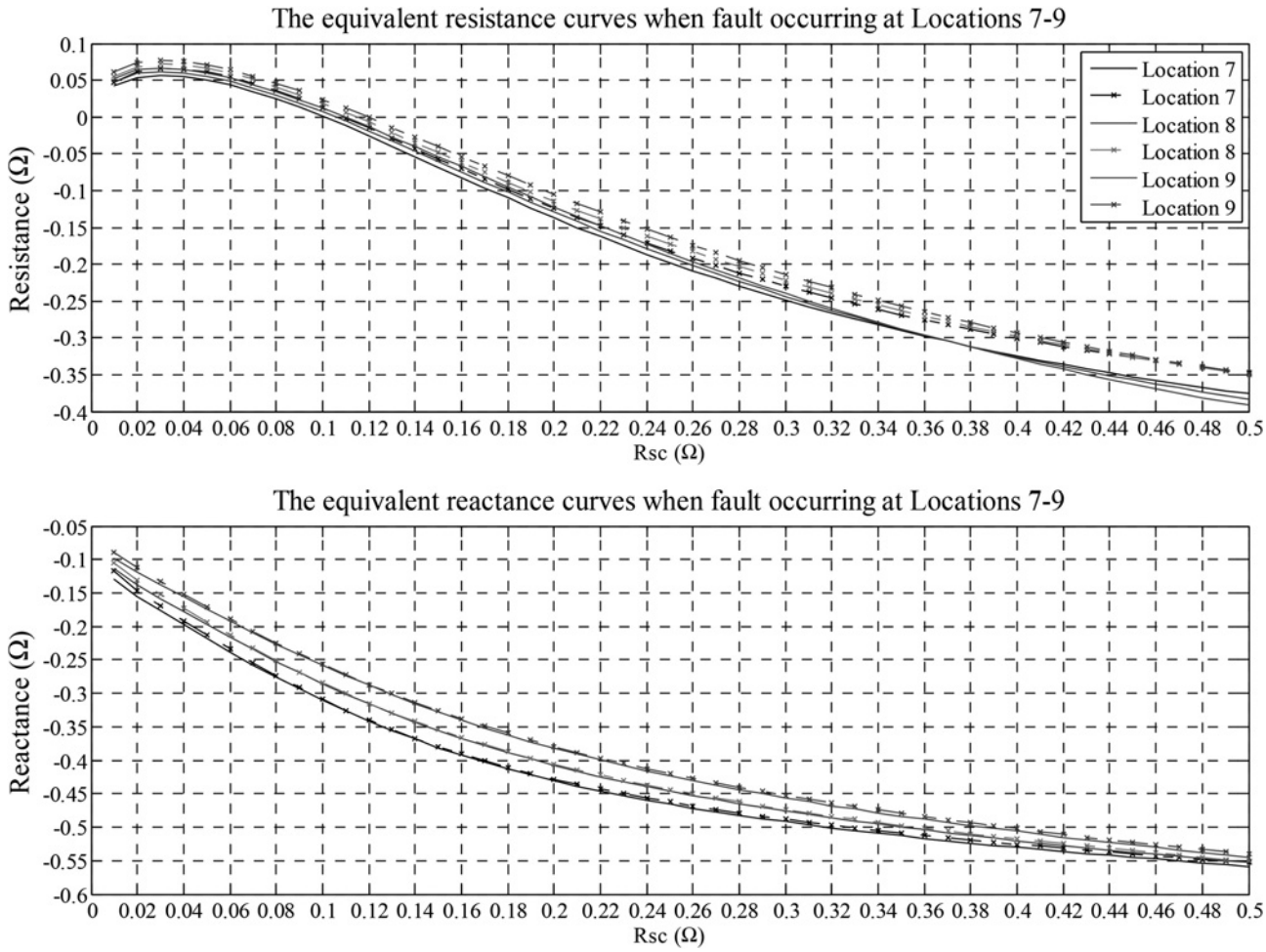

Fig. 15 *Equivalent impedance curves obtained at Load 3 when fault occurring at Locations 7–9 (solid line, results from the simulation; dash dot with 'x' line, results from the mathematical analysis)*

5 Conclusions

The mathematical analysis of the third harmonic currents produced by the diode bridge rectifier agrees with the simulation results. The line–line self-impedances at the harmonic frequencies are mathematically proven to be dependent on fault location and fault resistors. The agreements of the line–line self-impedances at the third harmonic frequency defined at each load from the mathematical analysis and the simulation method verify the effectiveness of this algorithm. If all parameters in a proposed aircraft system are known, the line–line self-impedance curves against fault location and fault resistor for each load can be predicted. The combination of the equivalent impedances for each load may be used to identify asymmetrical faults (phase–phase short-circuit) occurring on certain cable sections within the system. These results are consistent with the experimental study given in [16].

6 References

1 Rosero, J.A., Ortega, J.A., Aldabas, E., Romeral, L.A.R.L.: 'Moving towards a more electric aircraft', *IEEE Aerosp. Electron. Syst. Mag.*, 2007, **22**, pp. 3–9

2 Avery, C.R., Burrow, S.G., Mellor, P.H.: 'Electrical generation and distribution for the more electric aircraft'. Proc. 42nd Int. Universities Power Engineering Conf., 2007, (UPEC 2007), 2007, pp. 1007–1012

3 Emadi, K., Ehsani, M.: 'Aircraft power systems: technology, state of the art, and future trends', *IEEE Aerosp. Electron. Syst. Mag*, 2000, **15**, pp. 28–32

4 Tumilty, R.M., Brucoli, M., Burt, G.M., Green, T.C.: 'Approaches to network protection for inverter dominated electrical distribution systems'. Proc. Third IET Int. Conf. on Power Electronics, Machines and Drives, 2006, 2006, pp. 622–626

5 Ke, J., Thomas, D., Sumner, M.: 'A new single-ended fault-location scheme for utilization in an integrated power system', *IEEE Trans. Power Deliv.*, 2013, **28**, pp. 38–46

6 Hughes, M.B., Leonard, R.W., Martinich, T.G.: 'Measurement of power system subsynchronous driving point impedance and comparison with computer simulations', *IEEE Trans. Power Appar. Syst.*, 1984, **PAS-103**, pp. 619–630

7 Czarnecki, L.S., Staroszczyk, Z.: 'On-line measurement of equivalent parameters of distribution system and its load for harmonic frequencies'. Proc. IEEE 'Integrating Intelligent Instrumentation and Control' Instrumentation and Measurement Technology Conf., 1995, (IMTC/95), 1995, pp. 692

8 Czarnecki, L.S., Staroszczyk, Z.: 'On-line measurement of equivalent parameters for harmonic frequencies of a power distribution system and load', *IEEE Trans. Instrum. Meas.*, 1996, **45**, pp. 467–472

9 Wilsun, X., Ahmed, E.E., Xiqin, Z., Xian, L.: 'Measurement of network harmonic impedances: practical implementation issues and their solutions', *IEEE Trans. Power Deliv.*, 2002, **17**, pp. 210–216

10 Rizy, D.T., Gunther, E.W., McGranaghan, M.F.: 'Transient and harmonic voltages associated with automated capacitor switching on distribution systems', *IEEE Trans. Power Syst.*, 1987, **2**, pp. 713–72

11 Nagpal, M., Xu, W., Sawada, J.: 'Harmonic impedance measurement using three-phase transients', *IEEE Trans. Power Deliv.*, 1998, **13**, pp. 272–277

12 Ahmed, E., Xu, W., Liu, X.: 'Application of modal transformations for power system harmonic impedance measurement', *Int. J. Electr. Power Energy Syst.*, 2001, **23**, pp. 147–154

doi: 10.1049/iet-est.2011.0056

13 Yao, X., Maun, J.C., Mahmoud, H.B., Detroz, T., Stephane, D.: 'Harmonic impedance measurement using voltage and current increments from disturbing loads'. Proc. Ninth Int. Conf. on Harmonics and Quality of Power, 2000, 2000, vol. 1, pp. 220–225

14 Qian, Z., Sumner, M., Thomas, D.: 'Fault detection for aircraft power systems using the impedance at third harmonic frequency'. IET Ninth Int. Conf. on Developments in Power System Protection, 2008, (DPSP 2008), 2008, pp. 257–262

15 Qian, Z., Sumner, M., Thomas, D.: 'Fault detection for the aircraft distribution systems using impedance estimation'. Proc. Fourth IET Conf. on Power Electronics, Machines and Drives, 2008, (PEMD 2008), 2008, pp. 666–670

16 Zhou, Q., Sumner, M., Thomas, D.: 'Fault location for aircraft distribution systems using harmonic impedance estimation', *IET Electr. Syst. Transp.*, 2012, **2**, pp. 119–129

17 De Haan, S.W.H.: 'Analysis of the effect of source voltage fluctuations on the power factor in three-phase controlled rectifiers', *IEEE Trans. Ind. Appl.*, 1986, **IA-22**, pp. 259–266

18 Sakui, M., Fujitac, H., Shioya, M.: 'A method for calculating harmonic currents of a three-phase bridge uncontrolled rectifier with DC filter', *IEEE Trans. Ind. Electron.*, 1989, **36**, pp. 434–440

19 Sakui, M., Fujita, H.: 'Calculation of harmonic currents in a three-phase convertor with unbalanced power supply conditions', *IEE Proc. B*, 1992, **139**, pp. 478–484

20 Marouchos, C.C., Engineers, I.o.E.: 'The switching function: analysis of power electronic circuits' (The Institution of Engineering and Technology, 2006)

7 Appendix

7.1 Expression of the admittance matrix $[\mathbf{Y}'_3]$

Owing to the non-linearities of diode rectifier, the current and voltage switching functions are applied to derive the relationship between the input voltages and input currents at the input terminal of the diode rectifier [20]. Therefore the relationship between them at the fundamental frequency can also be expressed in the form of admittance at the corresponding frequency, as noted as $[Y_{I3}]$. The finite inductance on the line takes effects on the change of current during the commutation period and results in the overlap. The overlap angle is also considered to derive the relationship between the input currents and input voltages

$$[Y_{I3}] = \frac{16}{(\pi/2)\times R_{\mathrm{dc}}}\begin{bmatrix} A_{11} & A_{12} & A_{13} \\ A_{13} & A_{11} & A_{12} \\ A_{12} & A_{13} & A_{11} \end{bmatrix} + \frac{K}{\left(R_{\mathrm{dc}} + \mathrm{j}2\omega\left(L_{\mathrm{dc}} + L_f\right)\right)}\begin{bmatrix} A_{21} & A_{22} & A_{23} \\ A_{22} & A_{23} & A_{21} \\ A_{23} & A_{21} & A_{22} \end{bmatrix} \tag{25}$$

where $K = ((32)/(\gamma(\pi/2)))\sin^3(\gamma/2)$, $\gamma = \cos^{-1}\left\{1 - \left(2\pi f L_{\mathrm{line}} I_d\right)/\left(\sqrt{3}V_{\mathrm{pm}}\right)\right\}$ is the overlap angle when the system is in normal service and diode rectifier is supplied by balanced voltages, $A_{11} = (1/2)\cos(\gamma/2)$, $A_{12} = (1/2)\cos(2\pi/3 - (\gamma/2))$, $A_{13} = (1/2)\cos((2\pi/3) + (\gamma/2))$, $A_{21} = -(1/4)\exp(-\mathrm{j}(\theta_1 + \theta_2 + (\gamma/2)))$, $A_{22} = -(1/4)\exp(-\mathrm{j}(\theta_1 + \theta_2 + (\gamma/2) + (2\pi/3)))$ and $A_{23} = -(1/4)\exp(-\mathrm{j}(\theta_1 + \theta_2 + (\gamma/2) + (4\pi/3)))$. For the coefficients A_{21}, A_{22} and A_{23}, the parameters θ_1 and θ_2 are calculated as $\theta_1 = (\pi/6) - \varphi_0$ and $\theta_2 = \theta_1 + (2\pi/3)$. φ_0 is the initial phase angle of the phase voltage V_a.

The three-phase admittance matrix denoted as $\mathbf{Y}'_3$ is then described as in (26)

$$[\mathbf{Y}'_3] = [Y_{I3}]\left([Y_{T3}] + [Y_{I3}]\right)^{-1}[Y_{T3}] \tag{26}$$

7.2 Elimination of load currents in Section 3

In Section 1 of Section 3, load currents are eliminated. Here, how the load currents are eliminated is presented. Take Case 1 as example. The fault occurs on the cable section between Load 1 and the source terminal (Fig. 16).

According to Kirchoff's circuit law and node equations, the following expressions are obtained

$$[i_0] = [i_1] + [i_f] \tag{27}$$

$$[\boldsymbol{v}_0] - [\boldsymbol{v}_f] = [Z_{1f0}]\,[i_0] \tag{28}$$

$$[\boldsymbol{v}_f] - [v_1] = [Z_{1f1}]\,[i_1] \tag{29}$$

$$[\boldsymbol{v}_f] = [Z_f]\,[i_f] \tag{30}$$

$$[v_1] = [Z_1]\,[i_1] \tag{31}$$

Using (29)–(31), the fault currents and phase voltages at fault location can be expressed in terms of load current $[i_1]$ as in (32).

$$\begin{cases} [i_f] = [\boldsymbol{Y}_f]\left([Z_1] + [Z_{1f1}]\right)[i_1] \\ [\boldsymbol{v}_f] = \left([Z_1] + [Z_{1f1}]\right)[i_1] \end{cases} \tag{32}$$

In a similar way, the current $[i_0]$ can be expressed in terms of load current $[i_1]$ as in (33) by combining (27) and (32).

$$[i_0] = \left\{I + [Y_f]\left([Z_1] + [Z_{1f1}]\right)\right\}[i_1] \tag{33}$$

Combining (28), (32) and (33), the current flowing to Load 1 as noted as $[i_1]$ can be expressed in terms of the phase voltages at the source terminal $[\boldsymbol{v}_0]$ as in (34).

$$[i_1] = \left\{\left([Z_1] + [Z_{1f1}]\right) + [Z_{1f0}] + [Z_{1f0}]\,[\boldsymbol{Y}_f]\left([Z_1] + [Z_{1f1}]\right)\right\}^{-1}[\boldsymbol{v}_0] \tag{34}$$

In a similar way, currents flowing to Load 2 and Load 3 as noted as $[i_2]$ and $[i_3]$ can be expressed in terms of phase voltages at the source terminal $[v_0]$ in (35).

$$\begin{aligned} [i_2] &= \left\{[Y_2]\left([Y_2] + [Y_{T2}]\right)^{-1}[Y_{T2}]\right\}[\boldsymbol{v}_0] = [\boldsymbol{Y}'_2]\,[\boldsymbol{v}_0] \\ [i_3] &= \left\{[Y_{I3}]\left([Y_{I3}] + [Y_{T3}]\right)^{-1}[Y_{T3}]\right\}[\boldsymbol{v}_0] = [\boldsymbol{Y}'_3]\,[\boldsymbol{v}_0] \end{aligned} \tag{35}$$

Rewrite (1) in Section 3.1 in terms of source phase $[v_s]$ and

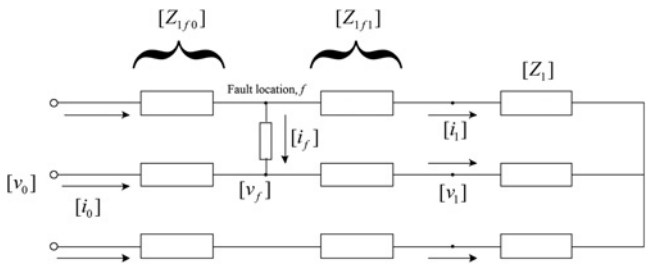

Fig. 16 *Example – fault occurs on the cable section between the source terminal and Load 1*

doi: 10.1049/iet-est.2011.0056

source impedance $[Z_s]$ as in (36)

$$[Z_s]^{-1}\left([v_s]-[\boldsymbol{v}_0]\right)=[i_1]+[i_2]+[i_3]+[i_f] \quad (36)$$

Substituting currents on the right-hand side of (36) with expressions (33)–(35), the phase voltages at the source terminal can be achieved as in (3).

If a fault occurs on the cable section between Load 2 and the source terminal, the three-phase admittance matrix $[\boldsymbol{Y}'_1]$ in (4) can be achieved in a similar way

$$[\boldsymbol{Y}'_1]=[Y_1]\left([Y_1]+[Y_{T1}]\right)^{-1}[Y_{T1}] \quad (37)$$

doi: 10.1049/iet-est.2011.0056